Journal of Alloys and Compounds 509 (2011) 4944–4949

Contents lists available at ScienceDirect

Journal of Alloys and Compounds

journal homepage: www.elsevier.com/locate/jallcom

Supplementary measurements of the primary crystalline phases of the Co–Ni–Sb and the Co–Fe–Sb ternary systems

Yubi Zhang[a,b], Changrong Li[a,*], Zhenmin Du[a], Cuiping Guo[a], Junqin Li[c], Miao Liu[a,d]

[a] School of Materials Science and Engineering, University of Science and Technology Beijing, Xueyuan Road 30#, Haidian District Beijing 100083, China
[b] Chongqing Instrument Materials Research Institute, Chongqing 400700, China
[c] College of Materials Science and Engineering, Shenzhen University, Shenzhen 518060, China
[d] Institute of Chemical Defense of PLA, Beijing 102205, China

ARTICLE INFO

Article history:
Received 30 September 2010
Received in revised form 19 January 2011
Accepted 20 January 2011
Available online 2 February 2011

Keywords:
Liquidus projection
The Co–Ni–Sb system
The Co–Fe–Sb system
As-cast solidification

ABSTRACT

Some primary crystalline phases of the Co–Ni–Sb and the Co–Fe–Sb systems are studied on the basis of the crystalline structure analysis by X-ray diffraction (XRD), the microstructure observation by scanning electron microscopy (SEM), the composition determination by electron probe microanalysis (EPMA) and the phase equilibrium relations of the constituent binary systems. From the experimental measurements of the present work and the phase equilibrium relations of literature reports, the liquidus projections of the Co–Ni–Sb and the Co–Fe–Sb ternary systems are determined. There exist 6 primary crystalline phases in each of the ternary systems, which are γ(A1)–Fcc_A1, β(Co,Ni)$_3$Sb–D0$_3$, γ(Co,Ni)Sb–NiAs, ζ(Co,Ni)Sb$_2$–FeS$_2$, η(Co,Ni)Sb$_3$–CoAs$_3$ and Sb–Rhombo_A7 in the Co–Ni–Sb system and γ(A1)–Fcc_A1, α(A2)–Bcc_A2, γ(Co,Fe)Sb–NiAs, ζ(Co,Fe)Sb$_2$–FeS$_2$, η(Co,Fe)Sb$_3$–CoAs$_3$ and Sb–Rhombo_A7 in the Co–Fe–Sb system. Two of invariant reactions are proposed, which are the eutectic reaction L → γ(A1) + β(Co,Ni)$_3$Sb + γ(Co,Ni)Sb in the Co–Ni rich side of the Co–Ni–Sb system and the transition reaction L + γ(A1) → α(A2) + γ(Co,Fe)Sb in the Co–Fe rich side of the Co–Fe–Sb system.

1. Introduction

The intermetallic compounds of the Co–Ni–Sb and the Co–Fe–Sb ternary systems have been studied extensively as thermoelectric and lithium-ion battery anode materials. The $CoSb_3$-based compounds have the typical skutterudite structure and show good thermoelectric properties such as low lattice thermal conductivities and high power factors by doping Ni, Fe, Sn or rare earth elements [1–5]. Co, Ni and Sb are the important component elements of the Half-Heusler thermoelectric alloys [6–8]. The intermetallic compounds, $CoSb_2$ [9], $NiSb_2$ [10], $FeSb_2$ [11] and $CoSb_3$ [12,13], and the $CoFe_3Sb_{12}$ based multiphase materials [14] are investigated as lithium-ion battery anode materials in recent years for their large latent capacities. Therefore, the knowledge of the phase relations of the Co–Ni–Sb and the Co–Fe–Sb ternary systems are of fundamental importance to understanding Sb–based materials. The liquidus projections of these two systems are studied on the basis of the phase equilibrium relations from literature and the supplementary experimental measurements of the present work.

2. Literature information

To facilitate reading, the symbols to denote the phases in the Co–Ni–Sb and the Co–Fe–Sb ternary systems are listed in Table 1.

As for the Co–Ni–Sb system, Dudkin and Abrikosov [15] and Naud and Parijs [16] reported the partial isothermal sections in the range of about 50–100 at.%Sb at 813 K and 873 K respectively. Five single phase regions, γ, ζ_1, ζ_2, η and Sb, seven two-phase regions, Sb + η, Sb + ζ_2, η + ζ_1, η + ζ_2, γ + ζ_1, γ + η and γ + ζ_2, and three three-phase regions, Sb + η + ζ_2, η + γ + ζ_1 and η + γ + ζ_2 were indicated. The phase γ was proposed to form a continuous homogeneity solution along the entire 50at.%Sb iso-compositional line. Ishida et al. [17] examined the solubility of Sb in the Co–Ni alloys in the temperature range from 973 to 1373 K by means of EPMA. Three phases γ(A1), β and γ were detected, and one three–phase region γ(A1) + β + γ and three two-phase regions γ(A1) + β, γ(A1) + γ and β + γ were determined. The phase γ reaches equilibrium with the phase γ(A1) when Ni at.% <20, and the phase β appears above this Ni content.

For the Co–Fe–Sb system, Geller [18] firstly measured the liquidus projection and the isothermal section at 298 K by metallographic method. Five primary crystalline regions, γ(A1), α(A2), γ, ζ and Sb, were determined except the phase η. Recently Voisin et al. [19] measured the isothermal section of the Co–Fe–Sb system at 1423K, but the phase γ was not found and the phases γ(A1)

* Corresponding author. Tel.: +86 10 82377789; fax: +86 10 62333772.
E-mail address: crli@mater.ustb.edu.cn (C. Li).

0925-8388/$ – see front matter © 2011 Elsevier B.V. All rights reserved.
doi:10.1016/j.jallcom.2011.01.160

Table 1
The list of the symbols to denote the phases in the Co–Ni–Sb and the Co–Fe–Sb ternary systems.

Symbol	Phase description
L or Liq	Liquid
γ(A1)	Solid solution in the Co–Ni or the Co–Fe rich sides with Fcc_A1 structure
α(A2)	Solid solution in the Co–Fe rich side with Bcc_A2 structure
γ	Continuous solid solution of γ(CoSb) and γ(NiSb) or γ(CoSb) and γ(FeSb)
β	Terminal ternary solid solution from $\beta(Ni_3Sb)$
δ	Terminal ternary solid solution from $\delta(Ni_3Sb)$
θ	Terminal ternary solid solution from $\theta(Ni_5Sb_2)$
ζ	Linear stoichiometric compound of $\zeta CoSb_2$ and $\zeta FeSb_2$
ζ_1	Linear stoichiometric compound of $\zeta CoSb_2$ with partial Co substituted by Ni
ζ_2	Linear stoichiometric compound of $\zeta NiSb_2$ with partial Ni substituted by Co
η	Linear stoichiometric compound of $\eta CoSb_3$ with partial Co substituted by Ni or Fe
Sb	Pure Sb with little solubilities of Co and Ni or Fe

and α(A2) were not differentiated from each other. Amornpitoksuk et al. [20] reported three isoplethal sections along the compositional lines of 30 at.%Sb, $Co_{0.5}Sb_{0.5}$–$Fe_{0.56}Sb_{0.44}$ and 75 at.%Sb. All the ternary phases extended from the terminal binaries were reported, while the phase γ(A1) was not included in the isoplethal section of 30 at.%Sb [21]. No ternary compounds were found in all of the reported literatures.

According to the above experimental information, the sample alloys were designed in the present work. In the Co–Ni–Sb ternary system, three Sb-rich alloys, CNS1–CNS3, were prepared to study their solidification paths. And other three alloys, CNS4–CNS6, were selected to determine the mono-variant line between the regions of the primary crystalline phases α and β. In the Co–Fe–Sb ternary system, one Sb-rich alloy CFS1 and one Sb-poor alloy CFS4 were selected to determine the mono-variant lines between the regions of the primary crystalline phases ζ and γ and between those of γ and α. And other two alloys, CFS2 and CFS3, were prepared to study their solidification paths. The experimental alloy compositions of the Co–Ni–Sb and the Co–Fe–Sb systems in this study are listed in detail in Table 2.

3. Experimental procedure

Cobalt, antimony, iron and nickel with purity higher than 99.9% were used as starting materials. The ingredients of the alloys with different compositions in the Co–Ni–Sb or the Co–Fe–Sb ternary systems were put into quartz tubes, which were first evacuated to high vacuum and then sealed under high purity argon to avoid the weight lost of samples owing to the high volatility of antimony. The sealed materials were molten by high frequency induction and shaken to ensure homogenization. The same method was used to prepare the Co–Fe–Sb ternary and the Fe–Sb binary samples in literatures [20–23].

Finally, the samples, keeping the sealed state, were cooled slowly in furnace to obtain the primary crystalline phases.

The as-cast samples were characterized by scanning electron microscopy (SEM, S250Mk3, 20 kV) for the microstructure observation, by X-ray diffraction (XRD, MAC-M21X, CuKα, 40 kV/20 mA) for the crystalline structure analysis, and by electron probe microanalysis (EPMA-1600, 20 kV) for the composition determination. No impurity elements from quartz tube were detected in the present investigation.

Table 2
Chemical compositions and primary crystalline phases of the Co–Ni–Sb and the Co–Fe–Sb ternary alloys.

Alloy (#)	Nominal composition (at.%)	Primary crystalline phase	Phase composition (at.%)
CNS1	Co–15Ni–70Sb	γ	Co–29.15Ni–49.16Sb
CNS2	Co–20Ni–60Sb	γ	Co–28.93Ni–50.7 Sb
CNS3	Co–7Ni–65Sb	γ	Co–8.54Ni–50.68Sb
CNS4	Co–68Ni–22Sb	Eutectic structure	Co–58.95Ni–21.84Sb
CNS5	Co–63Ni–26Sb	β	Co–58.34Ni–27.02Sb
CNS6	Co–58Ni–30Sb	β	Co–63.85Ni–27.69Sb
CFS1	Co–10Fe–85Sb	ζ	Co–11.53Fe–65.85Sb
CFS2	Co–5Fe–75Sb	γ	Co–12.33Fe–49.15Sb
CFS3	Co–20Fe–60Sb	γ	Co–13.24Fe–49.52Sb
CFS4	Co–35Fe–30Sb	γ	Co–24.80Fe–48.26Sb

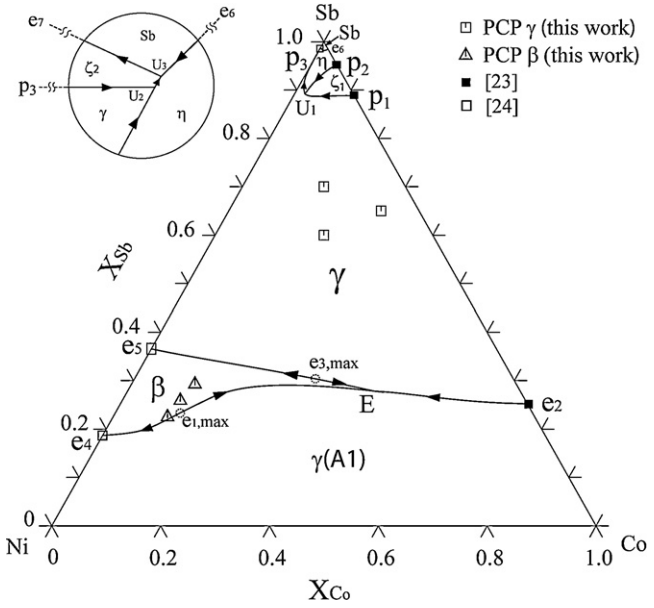

Fig. 1. Liquidus projection of the Co–Ni–Sb system.

4. Results and discussion

The liquidus projections of the Co–Ni–Sb and the Co–Fe–Sb systems are proposed, as shown in Figs. 1 and 2, based on the primary crystalline phase (PCP) relationship determined in this study together with the available information from literatures concerning the related binaries [24–28] and ternaries [18]. The primary crystalline phases in the alloys with different compositions deter-

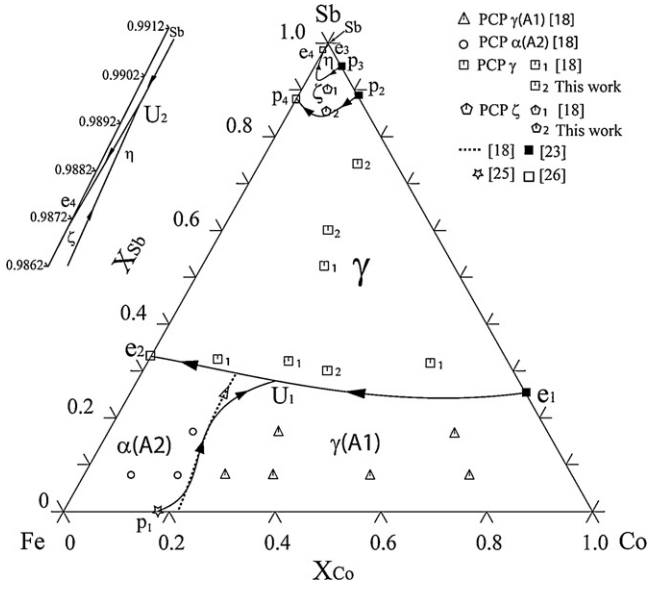

Fig. 2. Liquidus projection of the Co–Fe–Sb system.

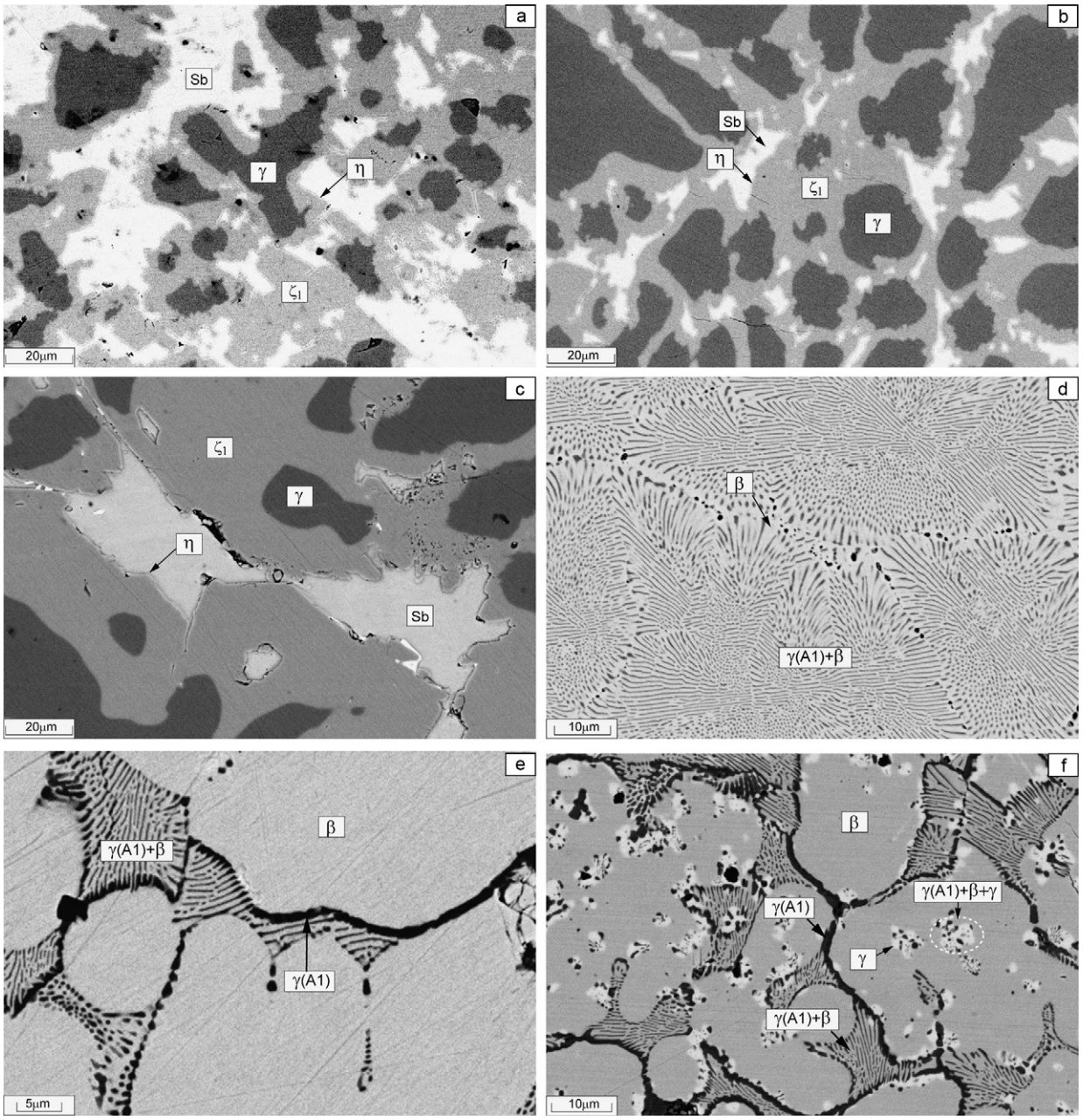

Fig. 3. SEM/BSE micrographs of the as-cast Co-Ni-Sb alloys. (a) CNS1 with XRD result $\gamma+\zeta_1+\eta+$Sb; (b) CNS2 with XRD result $\gamma+\zeta_1+\eta+$Sb; (c) CNS3 with XRD result $\gamma+\zeta_1+\eta+$Sb; (d) CNS4 with XRD result γ(A1)$+\beta$ and some low temperature phase δ; (e) CNS5 with XRD result γ(A1)$+\beta$ and some low temperature phase θ and δ; (f) CNS6 with XRD result γ(A1)$+\beta+\gamma$ and some low temperature phase θ.

mined in this study are summarized in the diagrams of the related liquidus projections.

Fig. 3a is the SEM/BSE micrograph of the alloy CNS1 (Co–15Ni–70Sb). The interdendritic morphology indicates that the black phase is the primary crystalline phase. The EPMA compositional analysis of the black phase is Co–21.95 at.%Ni–49.16 at.%Sb and presumes that the phase γ is a continuous solid solution composed of the binary phases γ(CoSb) and γ(NiSb). The SEM (Fig. 3a), EPMA (Table 2) and XRD (Fig. 4a) results together indicate the primary crystalline phase of the alloy CNS1 is the phase γ. After the formation of the primary crystalline phase γ, two consequent reactions may develop. One is the peritectic reaction between the liquid phase and the phase γ to form the phase ζ_1, $L+\gamma\rightarrow\zeta_1$. In micrograph, the phase ζ_1 is the grey phase formed around the primary crystalline phase γ. Afterwards, with the temperature descending, the solidification path passes through the primary crystalline surface of the phase ζ_1 and reaches the mono-variant reaction line between the primary crystalline surfaces of ζ_1 and η, where the other peritectic reaction occurs between the liquid phase and the phase ζ_1 to produce the phase η, $L+\zeta_1\rightarrow\eta$. The phase η is the very thin light grey phase around the phase ζ_1. Finally the liquid composition moves to the Sb corner and ends off solidification. The alloys CNS2(Co–20Ni–60Sb) and CNS3(Co–7Ni–65Sb) present similar results as shown in Fig. 3b and c but different ratios of phases. The XRD patterns of the alloys CNS1–3 are illustrated in Fig. 4a–c correspondingly.

Fig. 3d–f are the SEM/BSE micrographs of the alloys CNS4 (Co–68Ni–22Sb), CNS5 (Co–63Ni–26Sb) and CNS6 (Co–58Ni–30Sb). The micrograph of the CNS4 shows a nearly full eutectic γ(A1)$+\beta$ precipitation, suggesting that the alloy com-

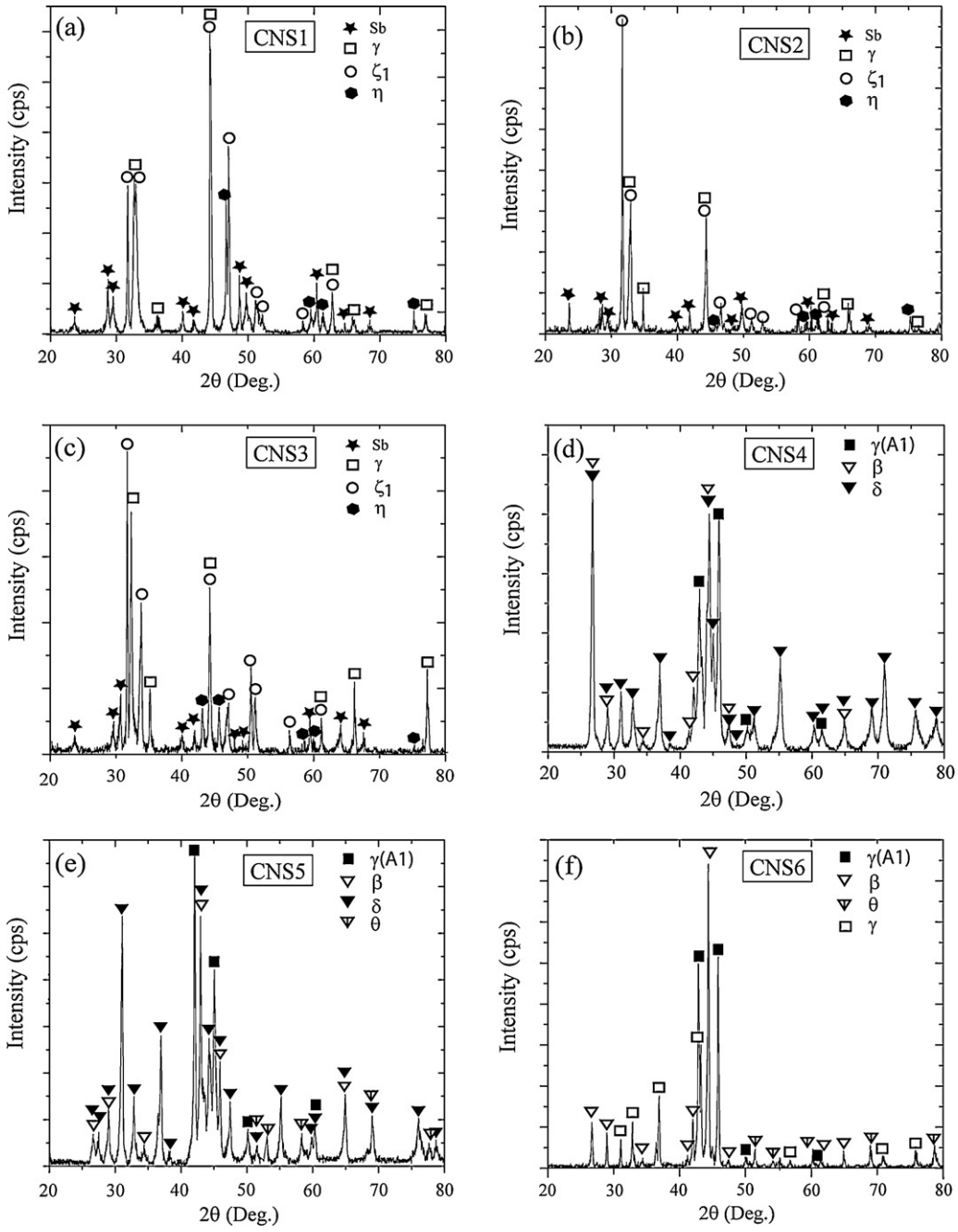

Fig. 4. XRD patterns of alloys in the as-cast condition and the identification symbols of phases. (a) CNS1; (b) CNS2; (c) CNS3; (d) CNS4; (e) CNS5; (f) CNS6.

position is close to the mono-variant reaction line of $L \rightarrow \gamma(A1) + \beta$, which is the intersection of the primary crystalline surfaces of γ(A1) and β. The solidification path goes forward along the mono-variant line towards to the terminal eutectic reaction e_4 of the Ni–Sb binary. The RXD analysis shows the existence of the phases γ(A1) and β together with a low temperature phase δ as shown in Fig. 4d. The phase δ is formed by the peritectoid transition $\gamma(A1) + \beta(Ni_3Sb) \rightarrow \delta(Ni_3Sb)$ starting from the Ni–Sb binary system, as shown in Fig. 5 [26].

With increasing the Sb content, in the alloy CNS5 the primary crystalline phase is the phase β as shown in Fig. 3e. Passing through the primary crystalline surface of the phase β, the liquidus composition reaches the mono-variant reaction line of $L \rightarrow \gamma(A1) + \beta$. The solidification path continues forward along the mono-variant line towards to the terminal eutectic reaction e_4 of the Ni–Sb binary. Two low temperature phases θ and δ exist in the sample which are identified by XRD pattern in Fig. 4e. Both phases θ and δ are formed by solid state transition as shown in Fig. 5.

With further increasing the Sb content, in the alloy CNS6 the primary crystalline phase is still the phase β as shown in Fig. 3f, but the solidification path changes direction, along the mono-variant reaction line of $L \rightarrow \gamma(A1) + \beta$ towards the ternary eutectic reaction E, $L \rightarrow \gamma(A1) + \beta + \gamma$, as shown in Fig. 1. The low temperature phase θ is detected by XRD analysis in Fig. 4f, which is formed by the solid phase transition from the high temperature phase β.

To summarize the information given in Fig. 1, the eutectic reaction $L \rightarrow \gamma(A1) + \beta(Co,Ni)_3Sb + \gamma(Co,Ni)Sb$ in the Co–Ni rich side of the Co–Ni–Sb system is proposed.

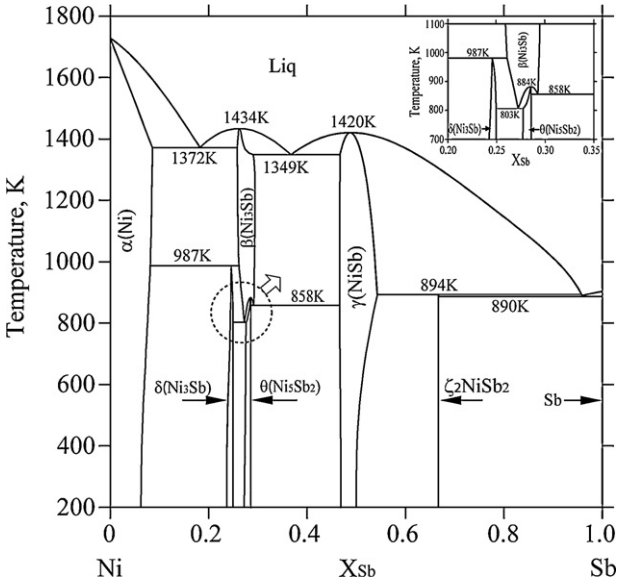

Fig. 5. The phase diagram of the Ni–Sb system.

For the Co–Fe–Sb alloys, the SEM/BSE micrographs and the XRD patterns of the alloys CFS1–4 are illustrated in Fig. 6a–d and Fig. 7a–d correspondingly. The SEM/BSE micrographs of the alloys CFS2 (Co–5Fe–75Sb) and CFS3 (Co–20Fe–60Sb) are similar as shown in Fig. 6b and c, which are analogous to those of the alloys CNS1–3 in Fig. 3a–c. The primary crystalline phase of the alloys CFS2 and CFS3 is the phase γ which is a continuous solid solution composed of the binary phases γ(CoSb) and γ(FeSb). As the formation of the primary crystalline phase γ, the solidification path reaches the mono-variant reaction line between the primary crystalline surfaces of γ and ζ, where the peritectic reaction $L+\gamma \rightarrow \zeta$ results in the formation of the phase ζ around the primary crystalline phase γ. With the temperature descending, the solidification path passes through the primary crystalline surface of the phase ζ and reaches the mono-variant reaction line between the primary crystalline surfaces of ζ and η, where the other peritectic reaction $L+\zeta \rightarrow \eta$ occurs between the liquid phase and the phase ζ to produce the phase η. The phase η is the very thin light grey phase around the phase ζ. Finally the liquid composition moves to the Sb corner and ends off solidification.

Fig. 6a is the micrograph of the alloy CFS1 (Co–10Fe–85Sb). Two phases ζ (grey) and Sb (white) are formed. The SEM, XRD and EPMA analyses indicate that the primary crystalline phase is the phase ζ. The solidification ends at the Sb corner.

Fig. 6d is the micrograph of the alloy CFS4 (Co–35Fe–30Sb). The primary crystalline phase is the phase γ according to the SEM, XRD and EPMA analyses. The solidification path crosses the primary crystalline surface of the phase γ and arrives at the mono-variant reaction line between the primary crystalline surfaces of γ and γ(A1) to form the eutectic structure $\gamma+\gamma$(A1).

The mono-variant line between the regions of the primary crystalline phases ε and α (i.e. α(A2) and γ(A1) in the present work) in the Co–Fe–Sb ternary system, proposed by Geller [18], was revised slightly in the present work, according to the Co–Fe binary phase diagram [27] in which the composition of the transition point p_1 (as shown in Fig. 2) is about 18 but not 22 at.%Co.

To summarize the information given in Fig. 2, the transition reaction $L+\gamma(A1) \rightarrow \alpha(A2)+\gamma$(Co,Fe)Sb in the Co–Fe rich side of the Co–Fe–Sb system is proposed.

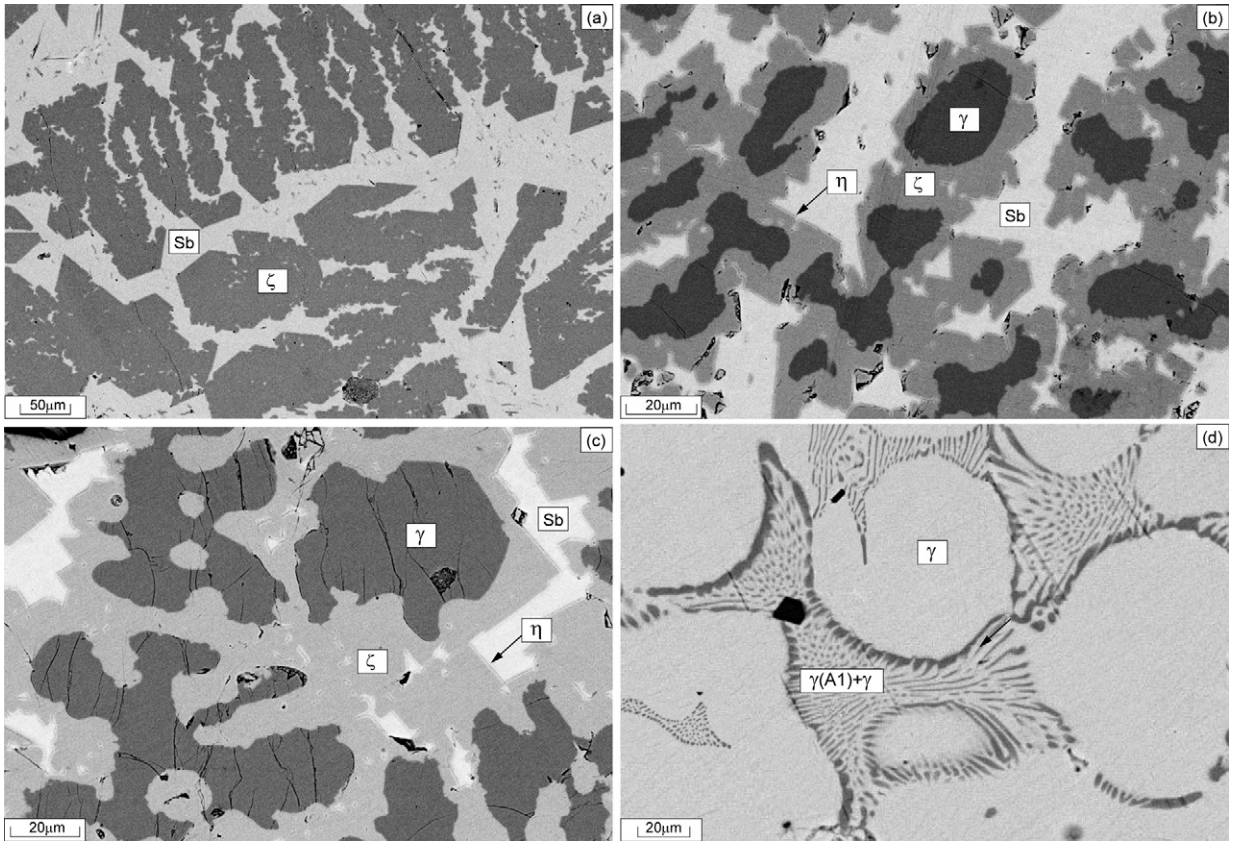

Fig. 6. SEM/BSE micrographs of the as-cast Co–Fe–Sb alloys. (a) CFS1 with XRD result ζ + Sb; (b) CFS2 with XRD result $\gamma+\zeta+\eta$ + Sb; (c) CFS3 with XRD result $\gamma+\zeta+\eta$ + Sb; (d) CFS4 with XRD result γ(A1) + γ.

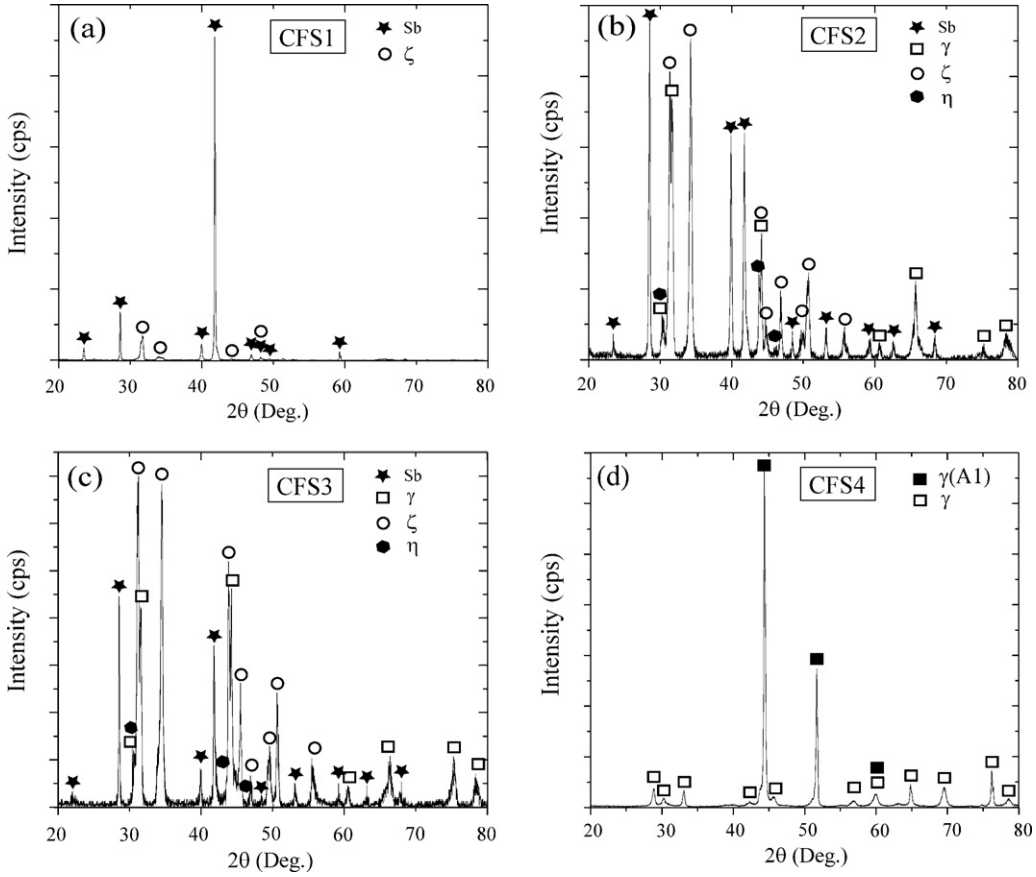

Fig. 7. XRD patterns of alloys CFS1–CFS4 in the as-cast condition and the identification symbols of the phases. (a) CFS1; (b) CFS2; (c) CFS3; (d) CFS4.

5. Conclusions

The as-cast samples of the Co–Ni–Sb and the Co–Fe–Sb systems are investigated by means of XRD, SEM and EPMA analyses. In all the tested samples, no ternary compounds are found. On the basis of the phase equilibrium relations from literatures and from the experimental measurements of the present work, the solidification path for each of the samples is studied. The primary crystalline phases and the liquidus surface projections of the Co–Ni–Sb and the Co–Fe–Sb systems are presented. Two of invariant reactions are proposed, which are the eutectic reaction $L \rightarrow \gamma(A1) + \beta(Co,Ni)_3Sb + \gamma(Co,Ni)Sb$ in the Co–Ni rich side of the Co–Ni–Sb system and the transition reaction $L + \gamma(A1) \rightarrow \alpha(A2) + \gamma(Co,Fe)Sb$ in the Co–Fe rich side of the Co–Fe–Sb system.

Acknowledgements

This work was supported by the National Natural Science Foundation of China (Nos. 50671009 and 50731002) and the National Doctorate Fund of the State Education Ministry of China (No. 20060008015).

References

[1] Y. Kawaharada, K. Kurosaki, M. Uno, S. Yamanaka, J. Alloys Compd. 315 (2001) 193–197.
[2] J.Y. Peng, J.Y. Yang, T.J. Zhang, X.L. Song, Y.H. Chen, J. Alloys Compd. 381 (2004) 313–316.
[3] K.T. Wojciechowski, Mater. Res. Bull. 37 (2002) 2023–2033.
[4] L. Bertini, C. Stiewe, M. Toprak, S. Williams, D. Platzek, A. Mrotzek, Y. Zhang, C. Gatti, E. Muller, M. Muhammed, M. Rowe, J. Appl. Phys. 93 (2003) 438–447.
[5] L. Yang, J.S. Wu, L.T. Zhang, J. Alloys Compd. 364 (2004) 83–88.
[6] K. Kawano, K. Kurosaki, T. Sekimoto, H. Muta, S. Yamanaka, Appl. Phys. Lett. 91 (2007) 62115–62118.
[7] M. Zhou, C.D. Feng, L.D. Chen, X.Y. Huang, J. Alloys Compd. 391 (2005) 194–197.
[8] V. Ponnambalam, B. Zhang, T.M. Tritt, S.J. Poon, J. Electron. Mater. 36 (2007) 732–735.
[9] J. Xie, X.B. Zhao, G.S. Cao, Y.D. Zhong, M.J. Zhao, J.P. Tu, Electrochim. Acta 50 (2005) 1903–1907.
[10] C. Villevieille, C.-M. Ionica-Bousquet, B. Ducourant, J.-C. Jumas, L. Monconduit, J. Power Sources 172 (2007) 388–394.
[11] J. Xie, X.B. Zhao, G.S. Cao, M.J. Zhao, Y.D. Zhong, L.Z. Deng, Mater. Lett. 57 (2003) 4673–4677.
[12] L.J. Zhang, X.B. Zhao, D.G. Xia, Mater. Lett. 59 (2005) 3448–3451.
[13] V. Pralong, J.-B. Leriche, B. Beaudoin, E. Naudin, M. Morcrette, J.-M. Tarascon, Solid State Ionics 166 (2004) 295–305.
[14] L.J. Zhang, X.B. Zhao, X.B. Jiang, C.P. Lv, G.S. Cao, J. Power Sources 94 (2001) 92–96.
[15] L.D. Dudkin, N.K. Abrikosov, Russ. J. Inorg. Chem. 2 (1957) 212–221.
[16] J. Naud, D. Parijs, Mater. Res. Bull. 7 (1972) 301–308.
[17] K. Ishida, M. Hasebe, N. Ohnishi, T. Nishizawa, J. Less-Common Met. 114 (1985) 361–373.
[18] W. Geller, Arch. Eisenhüttenwes 13 (1939) 263–266.
[19] L. Voisin, M. Hino, K. Itagaki, Shigen-to-Sozai 120 (2004) 131–135.
[20] P. Amornpitoksuk, H.X. Li, J.-C. Tedenac, S.G. Fries, D. Ravot, Intermetallics 15 (2007) 475–478.
[21] H. Ipser, K.W. Richter, Intermetallics 16 (2008) 119–120.
[22] D. Boa, S. Hassam, J. Rogez, K.P. Kotchi, J. Alloys Compd. 365 (2004) 228–232.
[23] K.W. Richter, H. Ipser, J. Alloys Compd. 247 (1997) 247–249.
[24] T. Nishizawa, K. Ishida, Bull. Alloy Phase Diagrams 4 (1983) 387–390.
[25] H. Okamoto, J. Phase Equilib. 12 (1991) 244–245.
[26] Y.B. Zhang, C.R. Li, Z.M. Du, C.P. Guo, Calphad 32 (2008) 378–388.
[27] T.B. Massalski, ASM Int. 2 (1990) 1186–1187.
[28] T.B. Massalski, ASM Int. 2 (1990) 1763–1767.